Wave energy converter arrays: Motion response of inter-connected array

Howey, B; Iglesias, G; Collins, KM; Hann, M; Greaves, D; Gomes, R; Henriques, JCC

Published in:
Host publication not specified in Elements

Publication date:
2019

Published in the Proceedings of the RENEW Conference, Lisbon, Portugal, October 2018:. In Advances in Renewable Energies Offshore - Proceedings of the 3rd International Conference on Renewable Energies Offshore, RENEW 2018 (pp. 625-632).

Wave Energy Converter Arrays: Motion response of inter-connected array

B. Howey[1], G. Iglesias[1] K.Collins[1] , M. Hann[1] , D. Greaves[1], R. Gomes[2] & J. Henriques[2]
1.Plymouth University, UK
2.IST, Portugal

ABSTRACT: Compact wave energy converter (WEC) arrays are a promising option in terms of optimizing energy output per unit area of marine space, realizing synergies in O&M tasks and auxiliary installations (substations, export cables, etc.), and achieving economies of scale. Four different levels of connectivity between five OWC spar buoys in a compact array – corresponding to as many mooring configurations – were tested in the Ocean Basin at the University of Plymouth. We find considerable implications of the inter-connectivity on the frequency of heave motion response, with interconnected cases yielding a higher natural frequency and an increase in magnitude compared to the baseline (non-connected) arrangement. This indicates the importance of a holistic inter-connected system design approach required in the early design stages with respect to the wave climate at the deployment site. For instance, for a site off Leixões (Portugal), the frequency upshift obtained through inter-connectivity may be beneficial.

1 INTRODUCTION

Climate change is a global issue with many challenges to be faced at a political, social and technical level. Multi-national agreements, such as the Paris Agreement and the Kyoto Protocol, are putting into place strict greenhouse gas (GHG) emission reduction targets (Paris Agreement, 2014). In order to achieve these targets and build a low-carbon economy, the European Commission formed the H2020 framework to tackle issues hindering progress in climate modelling and prediction, impact assessment, economics, funding and information networks and technology (H2020, 2014). Forming part of the last category, WETFEET was set up to address barriers to progress in the wave energy sector. Cost reduction through shared infrastructure has been highlighted as key breakthrough required to progress wave energy towards commercialisation (WETFEET, 2015). According to Thomsen et al (2018) mooring systems are listed as a key driver towards cost reduction in wave energy farm developments, estimated to compose 20–30% of the total structural costs. A large proportion of this cost is involved in anchorage. One solution to this is through the interlinking of devices within arrays to reduce the number of seabed anchors. It has been highlighted in many studies that the mooring system has a direct impact on the motion response, and therefore the performance, of a WEC (Johanning et al, 2007). This performance effect needs to be quantified in order to assess the possible cost benefit through the interlinking of devices. Previous physical studies (Falcao et al, 2015) have shown the interlinking of oscillating water column (OWC) devices improved array performance at higher frequencies, compared to an isolated device. It is difficult to isolate the array and interlinking effects on performance from Falcao et al (2015), as the results are relative to an isolated device, rather than an identical array with individual moorings. To assess this, the IST Spar-Buoy OWC, shown in Figure 2 was the candidate floating WEC used in these tests, using the most recent designs with an optimized geometry and mass distribution, as described by Ferreira (2016). This is an OWC type device that operates by extracting energy from the pressure differential resulting from the excitement of the water column acting as an air piston.

2 EXPERIMENTAL SETUP

Experiments were carried out in the Ocean Basin of University of Plymouth's COAST Lab. Waves were generated by 24 hinged flap absorbing paddles in a 35 x 15.5 m tank. The floor depth was set to 2 m, representing the scaled depth at the proposed deployment site of Leixões, Portugal.

2.1 *Mooring Layout*

To quantify the array effects, an isolated device was initially tested in a central position within the Ocean Basin. Subsequently, four arrays were tested (Figure 1).

- A Five individually moored devices
- B Five interconnected devices with eight seabed lines, four diagonals and four square connections
- C Five interconnected devices with four seabed lines, four diagonals and four square connections
- D Five interconnected devices with four seabed lines and four diagonal connections

From this point the following naming convention will be used to refer to particular devices within certain configurations:

$$TMx_{ARsi} \quad (4)$$

where *x* is a place holder for the device number, *A* is a placeholder indicating if the device is within an array (*A)* or isolated (*I)* configuration and (*B*) is a placeholder for the configuration. Subscripts *s* and *i* refer to the number of seabed lines and interconnections respectively. Square interlinks refer collectively to the lines in Configurations C and D connecting devices 1–2,1–4,4–5 and 2–5. Diagonal interconnections refer collectively to lines in Configurations B, C and D connecting the central to the outer devices (Figure 1).

2.2 *Decay Tests*

Free decay tests were performed in heave and surge in order to assess the natural characteristics of the central and a corner device of each configuration. A pulley system was used to initiate a displacement in the single degree of freedom of interest. Device positions were recorded using an infrared motion tracking system (Qualisys).

2.3 *Wave Conditions*

To establish device and array characteristics, regular waves were run at a constant wave height of H = 0.05 m, at frequencies between f = 0.3 Hz and f = 1.0 Hz, for 3 minutes (180 s). A frequency interval of 0.05 Hz was adopted, with extra frequencies tested around resonance. To establish the effect of any characteristic alterations induced by interlinking on operational performance, a set of three irregular conditions were run. The irregular states were based on the wave climate encountered at Leixões, Portugal and a Pierson Moskowitz spectrum was used. In order to make comparisons between the arrays, a constant significant wave height of H_{mo} = 0.05625 m was adopted and three peak periods of T_p = 1.2 s, 1.57 s and 1.93 s were used.

3 MODEL DESIGN AND BUILD

To create a 1:40 scale model with an appropriately scaled draught, the mass characteristics were amended to accommodate the freshwater in COAST Lab at the University of Plymouth. Geometric and Froude scaling were used to design 1:40 scale test models for use in the University of Plymouth's COAST lab. Scale models were built using off the shelf acrylic tube for the main float sections and OWC tube. The main ballast section at the base of the device, shown in yellow in Figure 2, was custom machined from aluminum. An orifice plate on top of the device simulated the power take off.

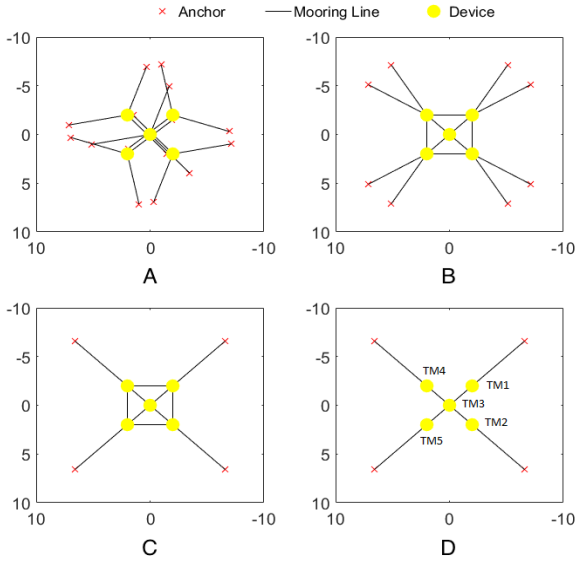

Figure 1 Mooring layouts for Configurations A–D.

To assess only the interlinking of the moorings, it was vital that the models were the same to avoid contamination of results. The mass, centre of gravity and pitch moment of inertia were all measured and compared to both the specification and to each other.

The devices were suspended horizontally from the ceiling by two lines and assumed to be axisymmetric. Load cells positioned within each line measured the forces in each line. Equating the moments on the system allowed for the calculation of the position of the centre of gravity (CoG). The total mass of the devices was measured as the sum of the loads measured in each line.

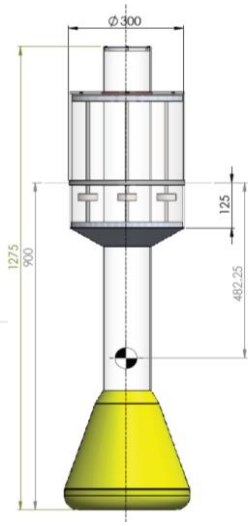

Figure 2 1:40 scale IST SparBuoy.

The pitch moment of inertia was measured using a swing test. The devices were suspended from a pivot at a distance from the CoG. A small displacement was induced, using a pulley system to limit the motion to a single degree of freedom and the device position was measured with an infrared motion tracking system. The natural frequency was calculated with a zero-crossing analysis of the resultant

motions, from which the moment of inertia was calculated in accordance with the methodology set out by Hirichsen (2014).

Table 1 shows that the measured masses were all within 1.5% of each other. This is further validated by the matching device draughts. The positions of the centre of gravity were all within 1% of one another. The I_{yy} moments of inertia were within 13% of one another; however, an uncertainty analysis of the measurement yielded an error of ±11% due to the measurement of the CoG position to the pivot point. Thus, the devices were considered similar and any differences were a result of array effects or mooring configuration.

Table 1. Positions of centre of gravity for each device and percentage difference from the CAD model.

Device	Mass [kg]	CoG [mm]	Draught [mm]	I_{yy} [kg m^2]
CAD	18.88	857.3	NA	3.83
TM1	18.74	867.7	890	3.40
TM2	18.75	862.8	890	3.40
TM3	18.93	859.1	890	3.92
TM4	19.02	859.9	890	3.69
TM5	18.77	862.6	890	3.69

4 MOORING DESIGN

The interconnected mooring system was designed to match the surge stiffness on the outer devices to that of the individually moored case, whilst minimizing the pre-tension.

Table 2. Mooring line properties for each configuration, where the mooring characteristics are described in Figure 3.

Config	B_c [m]	B_{cd} [mm]	B_{cl} [m]	B_{clp} [m]	B_f [g]	B_l [m]	S_{cl} [kg]	D_{cl} [kg]
A	1.16	4	1.81	1.29	5.00	5.01	NA	NA
B	1.93	6	0.31	2.38	25.0	5.63	0.16	0.39
C	2.68	6	0.80	1.81	35.0	4.31	0.17	0.38
D	3.40	6	0.53	2.13	45.0	3.59	NA	0.80

Chain sections were cut to length from stainless steel, with bar diameters indicated in Table 2. All clump weights were cylindrical bar sections of lead. The float mass was divided into five cylindrical sections (Figure 3) and cut from closed cell Styrofoam with a CNC hot wire. Mooring lines were cut to length from Dyneema rope and anchors were replicated by bolting the chain section to the basin floor. The characteristic B_{clp} relates to the distance between the fairlead and the connection of the clump weight on the seabed line and B_l, refers to the total length of Dyneema.

5 ANALYSIS METHODOLOGY

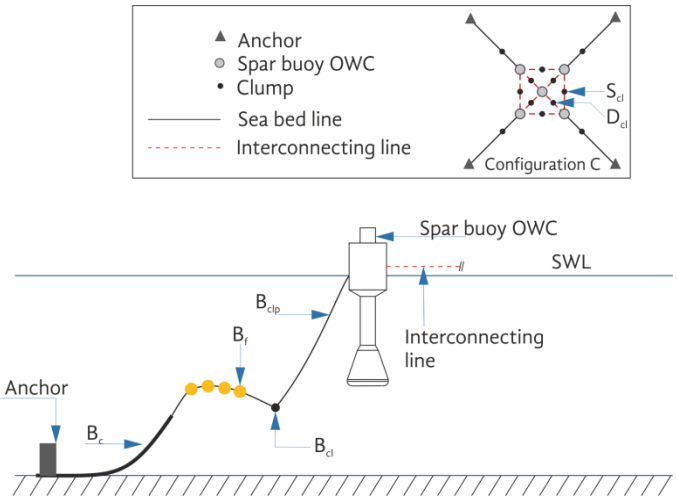

Figure 3 Naming conventions for mooring components.

5.1 *Decay tests*

A zero-crossing analysis was used to determine the natural period (T_0) of free decay response, with the natural frequency (f_0) being the reciprocal of the natural period. The system damping was calculated through the logarithmic decrement (Λ) as described in Eq. 5 and Eq. 6 (Ashton et al, 2009).

$$\Lambda = \ln\left(\frac{z(t)}{z(t+NT)}\right) N^{-1} \tag{5}$$

$$\xi_{tot} = \xi_0 + \xi_w + \xi_v = \frac{\Lambda}{T_0} \tag{6}$$

where ξ_{tot} is the total system damping, and subscripts 0, w and v denote the structural, radiation and viscous damping respectively.

5.2 *Motion*

Motion amplitude operators were derived to show linearized general responses for the isolated device and for the arrays of devices. For regular incident waves, this was calculated by dividing the amplitude of motion response $|X|$ by the amplitude of the measured incident wave A_w. For irregular cases, the quotient of the device displacement and the root mean square of the water surface elevation was used to represent the motion response operator (Eq. 7).

$$\sigma_x^* = \frac{\sigma_x}{\sigma_\eta} \tag{7}$$

where σ is the root mean square and subscripts x and η represent the degree of freedom of interest and the water surface elevation respectively.

6 RESULTS AND DISCUSSION

6.1 *Decay Tests*

In order to quantify the repeatability, tests were repeated three times. Repeats yielded a maximum difference in natural frequency of 1% for all heave tests. Surge results showed lower repeatability, especially for the interconnected cases, yielding up to 25% difference between tests. This was due to difficulty in restraining device pitching, which contaminated the results. Where repeats had a greater than 10% difference, results were ignored and replaced with NA in Table 3.

It appears from Table 3 that interlinking the devices shifted the heave natural frequency towards slightly higher frequencies for both the central and corner devices. Between the interlinked cases, there does not appear to be a great difference in the heave natural frequencies, suggesting that the level of connectivity did not make a significant difference to the array resonant frequencies. Again, there appears to be a circa 10% reduction in the heave damping values between the individually moored and interconnected arrays, but little difference between the interconnected arrays.

Table 3. Decay test results for array configurations

Device	Natural Frequency [Hz]		Damping [kg/m]	
	Heave	Surge	Heave	Surge
$TM3_{AA30}$	0.63	0.06	0.82	0.32
$TM2_{AA30}$	0.62	0.06	0.79	0.40
$TM3_{AB04}$	0.68	0.04	0.73	0.56
$TM2_{AB23}$	0.68	0.05	0.71	0.45
$TM3_{AC04}$	0.68	0.04	0.71	NA
$TM2_{AC13}$	0.68	0.04	0.67	NA
$TM3_{AD04}$	0.68	0.06	0.71	0.14
$TM2_{AD11}$	0.68	NA	0.71	NA

It can be seen from Table 3 that the surge natural frequency remains consistent across all configurations. This is due to the matching of the static stiffness to the isolated case in the early design stages, described in Section 4. Differences in the natural frequency and damping characteristics are attributed to dynamic effects. Table 3 shows a slight difference in the surge resonance of $TM3_{AD11}$ in Configuration D, where the natural period is shifted toward higher frequencies, similar to that of Configuration A. Due to the position of the fairlead with reference to the CoG, surge natural frequencies and damping characteristics were difficult to measure owing to contamination from motion in secondary degrees of freedom, namely pitch. As a result, some data is missing and marked NA in Table 3.

6.2 *Regular Motion Response*

The array effects on the largest motion responses are indicated by comparing the isolated device and the central device of Configuration A, as shown in Figure 4. The surge response can be seen to be very similar between the two cases, indicating negligible array effects. The heave response shows little difference between the cases apart from at $f = 0.63$ Hz where the Configuration A device shows a sharp reduction. This frequency is a harmonic of the width of the array and the width of the basin, and so reflections are likely to be affecting the results. Interestingly, the isolated device appears to show a resonant peak at $f = 0.525$ Hz, a lower frequency than the decay test results indicate. Previous studies of floating OWC type WECS, show similar results of a double peaked heave response (Gomes et al 2015a, 2015b), suggesting that the OWC resonance induces a heave response in the system. The maximum natural frequency of the water column, F_c, can be estimated with the simple analytical approximation given in Eq. 9 (McCormick, 2007) and found to be in close proximity to this resonant peak:

$$F_c = \frac{1}{2\pi}\sqrt{\frac{g}{L_1}} = \frac{1}{2\pi}\sqrt{\frac{9.81}{0.9}} = 0.525\ Hz \qquad (9)$$

where L_1 is the device draft.

Previous numerical studies, accounting for the effective length, also show a similar OWC natural fre-

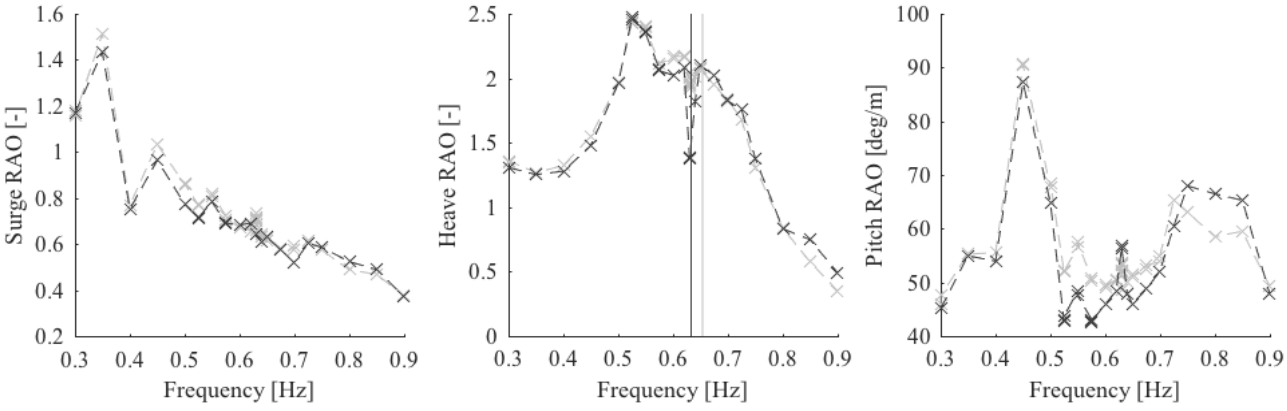

Figure 4 Motion response amplitude operators for an isolated TM3 device and the central device of Configuration A (TM3AA30) to show array effects.

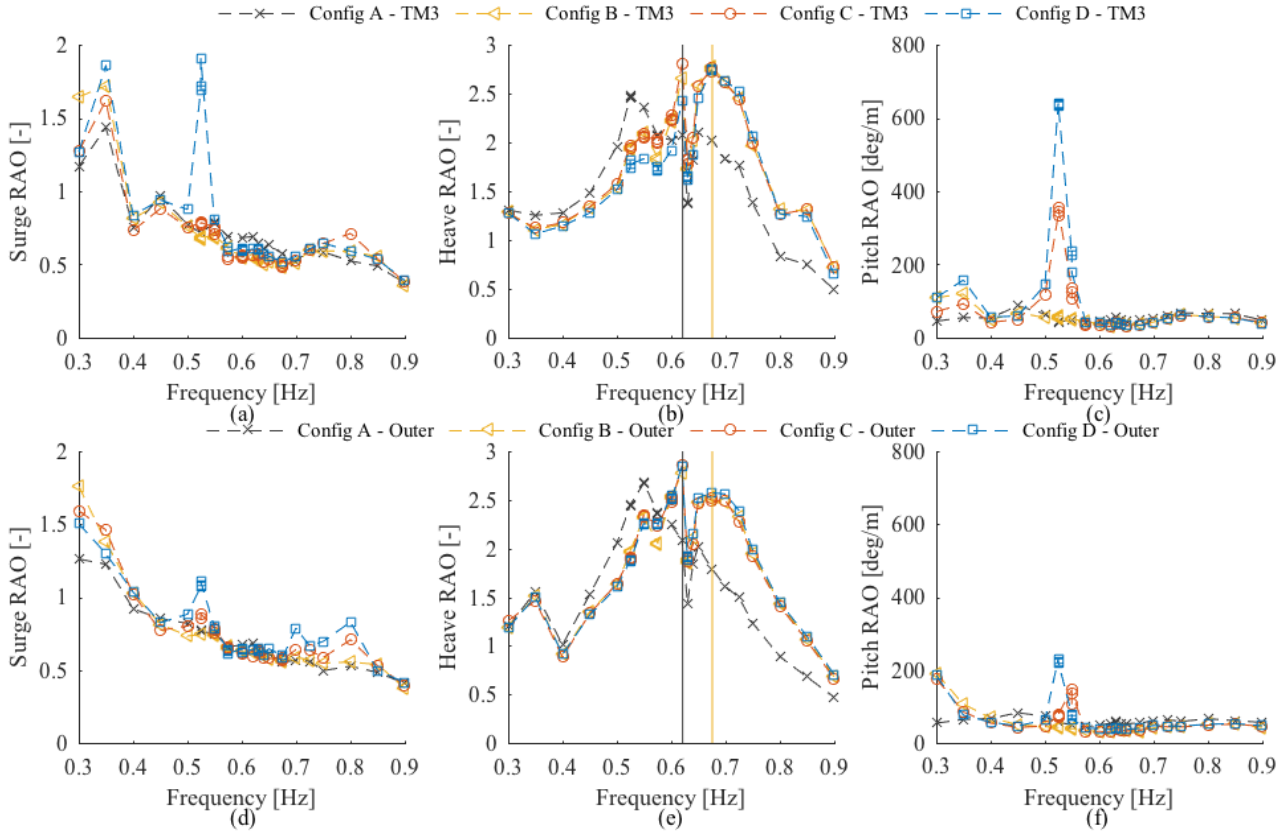

Figure 5 Response amplitude operators for the inner (a-c) and average motion response amplitude operators for the outer devices (d-f) of the arrays in all configurations. Vertical black and orange lines indicate the natural frequencies calculated from decay tests from configuration A and B respectively.

quency of 0.56 Hz (Collins et al, 2017). Interestingly, the OWC resonance appears to be inducing a greater heave response than at the body natural frequency as indicated by the heave decay tests for both the array and the isolated device. The largest rotational response was seen in pitch. The array is seen to have little effect on the pitch response, as seen in Figure 4**(**c).

In order to summarize the array configurations, the motion responses have been separated into outer (TM1, TM2, TM4, TM5) and inner devices (TM3) and averaged. Due to the large area being covered by the motion tracking system, accurate motion measurements of all devices were not possible. As a result, for this analysis TM1 has been ignored from the average in all configurations.

The main motion responses of the inner device and the average of the outer devices is shown in Figure 5(a-c) and Figure 5(d-f) respectively.

The general trends of both the inner (Figure 5(a)) and the outer (Figure 5(d)) show surge responses of similar magnitude and slope.

With reference to Figure 5(a), the surge response of the central device in all configurations appears to be similar except for a large peak for Configuration D at incident wave frequency f = 0.525 Hz. This is not seen in the outer devices to such an extent, Figure 5(d), suggesting that the removal of the square inter-connections reduces the surge constraint on the central device. Investigating the central device surge response time series at f = 0.525 Hz in the time and frequency domain, an underlying low-frequency response close to f = 0.2 Hz is evident. This frequency is very close to the pitch natural frequency and the incident wave frequency is close to the third harmonic, suggesting a strong coupling effect between the surge and pitch response. This seems intuitive as the fairlead connections are at a distance from the centre of gravity, resulting in a pitching moment on the device. This is supported by a large peak at the same frequency in the pitch response of Figure 5 (c).

The steep slope of the surge responses in Figure 5 (a) and Figure 5(d) indicates a frequency-dependence, but there is no global resonance peak within the frequencies tested for either the inner or outer device. This is concurrent with the findings of the surge decay tests (Table 1) where a peak would be expected below f = 0.3 Hz in all configurations.

A clear increase in heave is seen from all the interconnected cases at higher incident wave frequencies for both the inner and outer devices, shown in Figure 5(b) and in Figure 5(e). The magnitude of the increased response is similar for both the inner and outer devices. The decrease in heave response around f = 0.63 Hz is likely to be due to tank resonance, excited by the width of the array. To further support this theory, the numerical model created (Harnois et al 2018) that neglected the effects of the walls did not show this behaviour in any of the

simulations and the natural frequency matched that found in decay tests. Peaks in heave in all configurations, for both inner and outer devices, were apparent at f = 0.525 Hz; relating to the OWC resonance inducing a heave response of the device for both inner and outer devices. At lower incident wave frequencies, the interconnected cases appear to heave less than the individually moored case. A clear heave resonance shift towards f = 0.7 Hz can be seen in Figure 5(b) and Figure 5(e) for the interconnected configurations and can be attributed to the interconnections. This resonance shift is also supported by the WETFEET numerical model (Harnois et al, 2018) and the interconnected decay test results. In both Figure 5(b) and Figure 5(e) there appears to be a large body resonance response aligning with the decay test results at f = 0.675 Hz, although the tank wall effects may be masking a resonant peak at a slightly lower frequency. This body resonance F_z also falls within the simple approximations in Eq. 10 (McCormick, 2007) and computations using WAMIT of 0.69 Hz (Gomes et al, 2016).

$$F_z = \frac{1}{2\pi}\sqrt{\frac{\rho g A_{wp}}{m+m_w}} = 0.63 < \mathrm{F_z} > 0.88\ [Hz] \qquad (10)$$

where ρ is the water density, g is the acceleration due to gravity, A_{wp} is the area at the water plane, m is the device mass and m_w is the added mass.

The array effects noticed at high frequencies, shown in Figure 4(b), can be seen to be magnified by the interconnections in Figure 5(b), between f = 0.8 Hz and f = 0.9 Hz.

A significant difference can be seen between the magnitude of the pitch response of the inner (Figure 5(c)) and the outer (Figure 5(f)) devices, particularly in configuration C and D. Except at very low frequencies, Configurations A and B indicate a relatively constant pitch response regardless of positioning within the array.

Large peaks around f = 0.5 Hz in the pitch motion response of the inner devices are very clear in Configurations C and D (Figure 5(c)). As previously discussed, this is indicative of strong coupling between pitch and surge responses. The central device pitch response is significantly larger than the outer device, indicating that the interconnecting lines are providing a much lower restoring constraint at frequencies circa f = 0.525 Hz than the outer device mooring connections in Configurations C and D.

Interestingly, by removing a seabed line and moving to the single line from an outer device (Configuration B to C), the central device behaved very differently (Figure 5(c)). The single-point bottom line on the outer device allowed all devices to pitch significantly more than in Configuration B. This could have significant implications for energy extraction and line tensions.

6.3 *Irregular Motion Response*

Irregular motion responses, as calculated by Eq. 7, were calculated for each device within each configuration. The box plots in Figure 6 show the average and spread of device responses (neglecting TM1 for reasons previously stated) for each configuration at each value of T_p tested. In all modes of motion, apart from heave, Figure 6 suggests that an individually moored array behaves more homogeneously than interconnected cases, for which the magnitude of the motion in question varies spatially across the array.

There was a very noticeable difference between the interconnected and individually moored cases with regard to the surge response. The interconnections significantly reduced the constraint in surge across all peak periods tested. The magnitude of this response does not correlate to the responses plotted in Figure 5(a) and Figure 5(d), indicative of the magnitude of non-linear effects. A large difference between Configuration A and the interconnected cases is seen in Figure 6(a), that is not apparent in Figure 5(a) or Figure 5(d). This suggests that the interconnected arrays are more susceptible to non-linear effects.

A very clear difference between the interconnected and individually moored cases can be seen in the heave responses in Figure 6(c). The spatial differences in the heave response appear to be very similar for all cases. The interconnected cases seem to all have a similar heave response that is greater than the individually moored case in all the irregular cases tested. The spread of the heave responses appears to be similar for all configurations, suggesting that power outputs from the individually moored and interconnected cases should be spatially well-balanced. A significant difference in the mean heave of the individually moored and interconnected cases was seen across all periods tested, as in the regular cases. Depending on the phase of this response, one would expect this to result in an enhanced power output for the interconnected cases.

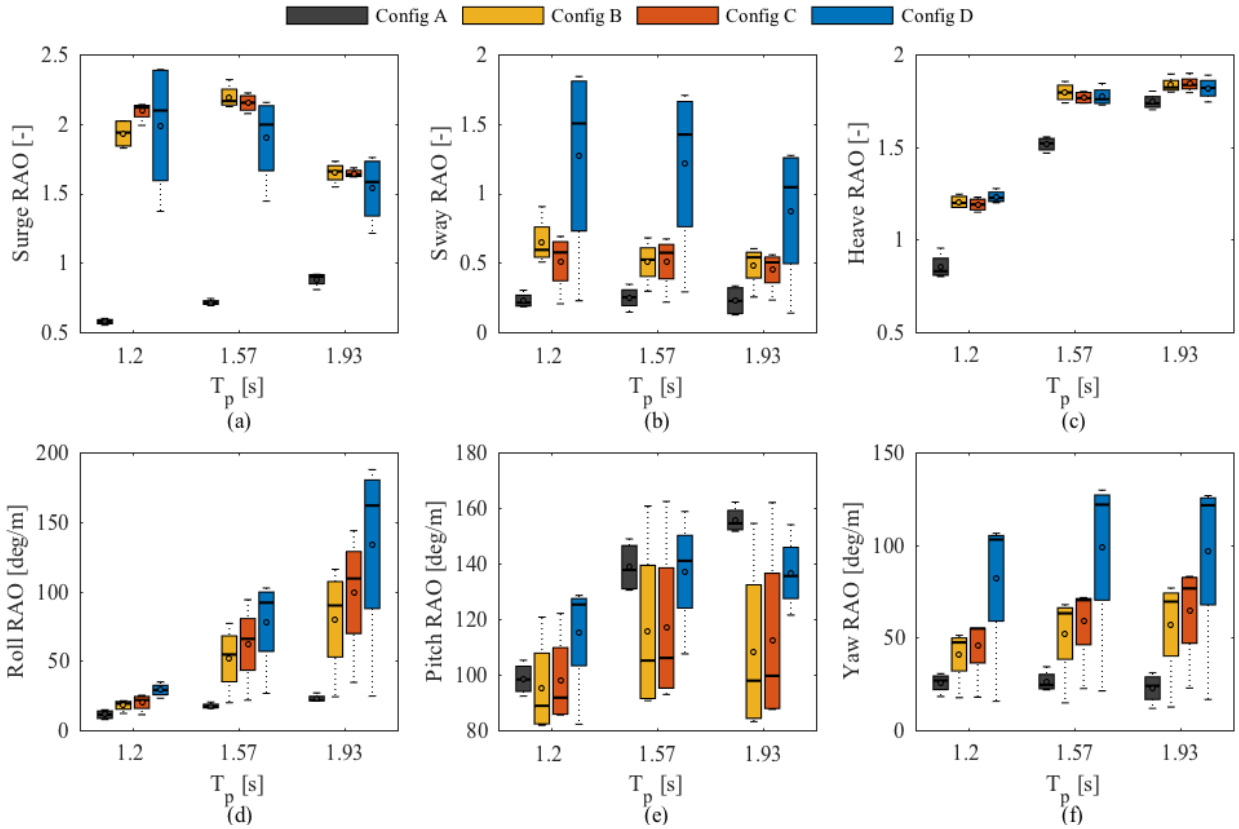

Figure 6 Box plots of irregular motion responses for all array configurations, with the inter quartile range as a shaded block, the mean as a 'o' marker and the median as horizontal line.

Between the interconnected cases, Configurations B and C seem to behave very similarly in all modes of motion with comparable averages and similar spatial variations. This suggests that moving from two bottom mooring lines to a single one, did not significantly affect the motions of arrays. For the case of Configuration D at T_p = 1.93 s, a slight decrease in average heave and an increase in average pitch was seen, which could cause sloshing of the water column, having implications relating to performance with respect to the other configurations. It appears from Figure 6 that the spatial homogeneity of the array motions is inversely proportional to the number of interconnections in most degrees of freedom. This is further highlighted in the increasing difference between the mean and median of responses in most degrees of freedom, as fewer interconnections are present. This demonstrates the importance for developers to consider individual device and mooring line optimization for devices within an interconnected array; more so than for a standard individually moored array.

7 CONCLUSIONS

Wave energy is an area of technology with great potential, but development in the sector is currently being slowed due to high costs. Moorings and installation costs were highlighted as a breakthrough by the WETFEET project (WETFEET, 2015), required to accelerate growth and encourage investment into the sector. This paper covered the implications of the interlinking of devices, and associated anchorage requirement reduction, within WEC arrays.

The interconnecting of devices has been shown to significantly alter the heave resonance characteristics of the arrays compared to its individually moored control array. The interconnections appear to shift the resonance towards higher frequencies, with the level of interconnection making very little difference. The spatial variation in motion response within an interconnected array has been shown to have an inverse relation with the number of interconnections.

The main conclusion from this paper is that interconnected WEC arrays require careful design, considering the interconnecting moorings at very early stages to optimise the design to a specific location. A developer cannot simply interconnect devices that are not specifically tuned for this purpose; the result of doing so may be a significantly sub-optimal design. This paper shows that the level of interconnection significantly alters the motion responses of the devices, particularly in the rotational degrees of freedom. Designers need to consider device positioning within an array when designing each interconnecting mooring line to optimize these types of array.

REFERENCES

Ashton, I.G., Johanning, L. and Linfoot, B., 2009, January. Measurement of the effect of power absorption in the lee of a wave energy converter. In ASME 2009 28th International Conference on Ocean, Offshore and Arctic Engineering (pp. 1021-1030). American Society of Mechanical Engineers.

Falcao, Antonio & Henriques, Joao. & Gomes, Rui & Vicente, Pedro. & Fonseca, Francisco. & Varandas, Jose. & Trigo, Luis. 2015. Dynamics of oscillating water column spar-buoy wave energy converters deployed in array and its survivability in extreme conditions. Marinet Infrastructure Access Report

Ferreira, J. 2016. Experimental study of the dynamic instability in the oscillating water column spar buoy. IST

Gomes, RPF & Henriques, JCC and Gato, LMC & Falco, AF de O. 2015a. Wave channel tests of a slack-moored floating oscillating water column in regular waves. Proceedings of the 11th European Wave and Tidal Energy Conference. France

Gomes, RPF & Henriques, JCC & Gato, LMC & Falco, AFO & Guedes Soares, C. 2015b. Testing of a small-scale model of a heaving floating OWC in a wave channel and comparison with numerical results. Renewable Energies Offshore (ed. C. Guedes Soares): 445-454

Gomes, RPF & Vicente, PC & Henriques, JCC & Gato, LMC. 2016. WP2 – System description for OWC and Symphony. WETFEET.

Harnois, V. & Collins, K. & Greaves, D. & Howey, B. & Gomes, R. & Portillo, J. & Vicente, P. & Vicente, M. 2017. D6.4 - Validated numerical simulation of hydrodynamic interaction between devices for different compact array layouts. WETFEET

Hirichsen, P.F., 2014. Bifilar suspension measurement of boat inertia parameters. Journal of Sailboat Technology, 1, pp.1-37.

H2020. 2014. Online. Available at: https://ec.europa.eu/programmes/horizon2020/what-horizon-2020 . Accessed 04 May 2018

Johanning, L. & Smith, G. & Wolfram, J. 2007. Measurements of static and dynamic mooring line damping and their importance for floating WEC devices. Ocean Engineering. 24. 14:1918 – 1934

McCormick, M.E. 2007. Ocean Wave Energy Conversion. Dover Publications

Paris Agreement. 2014. Online. Available at: http://unfccc.int/kyoto_protocol/items/2830.php Accessed 04 May 2018

Thomsen, J.B. & Ferri, F & Kofoed, J.P. & Black, K. 2018. Cost Optimization of Mooring Solutions for Large Floating Wave Energy Converters. Energies.11.1

WETFEET.2015. online. Available at: http://www.wetfeet.eu. Accessed 04 May 2018